CHEMISTRY OF MATERIALS

ARTICLE

pubs.acs.org/cm

Influence of the La/M Network on Magnetic Properties of Mn_4 Tetrahedra in Intermetallic Compounds $La_{21-\delta}Mn_8M_7C_{12}$ (M = Ge, Sn, Sb, Te, Bi)

Julia V. Zaikina,[†] Inga Schellenberg,[‡] Evan M. Benbow,[†,§] Rainer Pöttgen,[‡] and Susan E. Latturner*[,†]

[†]Department of Chemistry and Biochemistry, Florida State University, Tallahassee, Florida 32306, United States

[‡]Institut für Anorganische und Analytische Chemie, Universität Münster, 48149 Münster, Germany

Supporting Information

ABSTRACT: Crystals of $La_{21-\delta}Mn_8M_7C_{12}$ (M = main group elements Ge/Al, Sn, Sb, Te, Bi) were synthesized in La/Ni eutectic flux. The structure features tetrahedral manganese clusters edge-capped by carbon atoms, Mn_4C_6, embedded into a nonmagnetic La/M network. The structures were determined from single-crystal X-ray diffraction ($La_{21}Mn_8Ge_{6.2}Al_{0.8}C_{12}$, $Fm\bar{3}m$; a = 16.2259(3) Å; Z = 4; R_1 = 0.022). While most of the $La_{21}Mn_8M_7C_{12}$ analogues are completely ordered, the M = Te compound features partial occupancy of one of the La sites, and the M = Ge analogue exhibits mixed Ge/Al occupancy on one of the M sites. $La_{21-\delta}Mn_8M_7C_{12}$ with M = Sn, Sb, Te, Bi are paramagnets, but the susceptibility of $La_{21}Mn_8Ge_{6.2}Al_{0.8}C_{12}$ exhibits ZFC-FC divergence at $T_1 \approx 6$ K and an additional feature at $T_2 \approx 3$ K. Such behavior is indicative of frustration of antiferromagnetically coupled manganese magnetic moments within the Mn_4 tetrahedra. AC susceptibility measurements confirm the presence of two cusps at T_1 and T_2; however, no frequency dependence of cusp maxima was found. This differentiates $La_{21}Mn_8Ge_{6.2}Al_{0.8}C_{12}$ from the Fe analogue, $La_{21}Fe_8Sn_7C_{12}$, where frequency dependence indicates spin-glass behavior. Electronic calculations on $La_{21-\delta}Mn_8M_7C_{12}$ confirm that the vacancy on one of the La sites in the $La_{20}Mn_8Te_7C_{12}$ analogue stabilizes the phase by shifting the Fermi level to a pseudogap in the density of states. ^{57}Fe and ^{119}Sn Mössbauer spectroscopy of spin-glass compound $La_{21}Fe_8Sn_7C_{12}$ and paramagnetic $La_{21}Mn_8Sn_7C_{12}$ supports the presence of spin glass behavior in the Fe analogue and not in the Mn analogue.

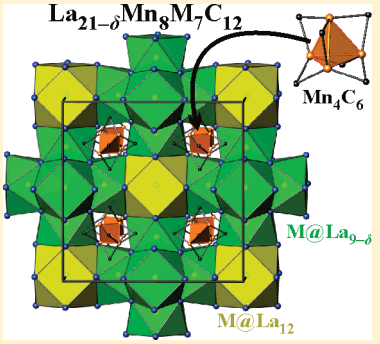

KEYWORDS: $La_{21}Fe_8Sn_7C_{12}$, La/Ni flux, flux growth, spin-glass, carbide, Mössbauer spectroscopy

INTRODUCTION

Ternary carbides of transition (T) and rare-earth (RE) metals $RE_xT_yC_z$ exhibit wide-ranging structural diversity associated with different connectivity within the zero-, one-, two-, or three-dimensional $[T_yC_z]^{n-}$ complex anions. Also diverse are the various types of carbon fragments, ranging from monatomic C_1 specimens to extended C_2 and C_3 units.[1] The recent extensive study of transition metal carbides is driven by their interesting physical properties, for example, superconductivity in $LaNiC_2$,[2] Y_2FeC_4,[3] and Sc_3CoC_4[4] and complex magnetic behavior in RE_2TC_2 (RE = Y, Ce−Nd, Gd−Tm; T = Re, Os).[5a] In most transition metal carbides the *d*-metals are either isolated from each other (d > 5 Å) or form infinite one or higher dimensional fragments. So despite the increasing number of multinary carbide phases, isolated clusters of transition metals are not a common building block in transition metal carbides. An interesting recent example is the planar Fe_6 cluster in $RE_{15}Fe_8C_{25}$ (RE = Y, Dy, Ho, Er).[5b]

Recently, the novel compound $La_{21}Fe_8M_7C_{12}$ was reported, featuring perfect tetrahedral iron clusters edge-capped by carbon atoms.[6] In its crystal structure, the Fe_4C_6 clusters are separated from each other and surrounded by a nonmagnetic La/M network (M = Ge/Al, Sn, Sb, Te/Al, Bi). Isolated tetrahedral clusters of magnetic atoms with equal antiferromagnetic (AFM) exchange coupling is an example of an ideal spin-frustrated system with a highly degenerate magnetically ordered ground state and is of particular interest as a "toy problem" in computational chemistry.[7] The compound $La_{21}Fe_8Sn_7C_{12}$ exhibits spin-glass behavior associated with frustration of antiferromagnetically coupled iron moments within the perfect Fe_4 tetrahedra. This phase was synthesized utilizing an unconventional flux, La/Ni eutectic (mp 532 °C),[8] which has proven to be an excellent growth medium for preparation of millimeter size crystals of phases containing carbon, boron, and transition metals.[6,9]

In this work we extended the study of phases with isolated T_4C_6 clusters to T = Mn; this metal shows structural trends and reactivity in La/Ni eutectic flux similar to iron. The new quaternary carbides $La_{21-\delta}Mn_8M_7C_{12}$ (M = Ge/Al, Sn, Sb, Te, Bi) are isostructural to $La_{21}Fe_8M_7C_{12}$.[6] Their crystal structure peculiarities, electronic structure, and magnetic properties

Received: October 3, 2010
Revised: January 31, 2011
Published: March 11, 2011

Table 1. Data Collection and Structure Refinement Parameters for $La_{21-\delta}Mn_8M_7C_{12}$[a]

composition	$La_{21}Mn_8Sn_7C_{12}$ (I)	$La_{21}Mn_8Bi_7C_{12}$ (II)	$La_{21}Mn_8Sb_7C_{12}$ (III)	$La_{21}Mn_8Ge_{6.2}Al_{0.8}C_{12}$ (IV)	$La_{20.02(1)}Mn_8Te_7C_{12}$ (V)
space group			$Fm\bar{3}m$ (No. 225)		
collection temperature, K			295 K		
cell parameter, *a*, Å	16.7435(2)	16.6072(5)	16.4829(4)	16.2259(3)	16.4455(7)
V, Å^3	4694.0(1)	4580.3(2)	4478.2(2)	4272.0(1)	4447.8(3)
Z			4		
density (calcd), g cm^{-3}	6.13	7.20	6.46	6.18	6.36
μ, mm^{-1}	24.3	48.0	25.8	27.0	25.4
data collection range, deg	4−30	2−35	2−35	2−32	2−35
absorption type	numerical	numerical	numerical	multiscan	numerical
reflections collected	8892	11166	11350	9045	12751
independent reflections	391 [R_{int} = 0.060]	566 [R_{int} = 0.064]	556 [R_{int} = 0.038]	412 [R_{int} = 0.047]	553 [R_{int} = 0.031]
parameters refined	21	21	21	22	21
R_1[b]	0.018	0.019	0.018	0.020	0.023
wR_2[c] [$F_o > 4\sigma F_o$]	0.037	0.037	0.038	0.042	0.045
R_1, wR_2 (all data)	0.022, 0.038	0.022, 0.038	0.019, 0.038	0.022, 0.043	0.032, 0.047
largest diff. peak and hole, e/Å^3	2.64 and −1.03	1.30 and −1.07	1.03 and −1.04	1.25 and −1.33	2.29 and 1.72
goodness-of-fit	1.085	1.243	1.384	1.187	1.055

[a] Further details of the crystal structure determination may be obtained from Fachinformationszentrum Karlsruhe, D-76344 Eggenstein-Leopoldshafen, Germany, on quoting the depository numbers CSD-422157, CSD-422154, CSD-422156, CSD-422155, and CSD-422153 for I, II, III, IV, and V, respectively. [b] $R_1 = \Sigma||F_o| - |F_c||/\Sigma|F_o|$. [c] $wR_2 = [\Sigma w(F_o^2 - F_c^2)^2/\Sigma w(F_o^2)^2]^{1/2}$, $w = [\Sigma^2(F_o^2) + (A\cdot p)^2 + B\cdot p]^{-1}$; $p = (F_o^2 + 2F_c^2)/3$; A = 0.0061 (I), 0.0037 (II), 0.006 (III), 0.0118 (IV), 0.0156 (V); B = 169.5289 (I), 105.1632 (II), 101.1289 (III), 153.3339 (IV), 91.9764 (V).

were explored using X-ray diffraction, magnetic susceptibility measurements, Mössbauer spectroscopy, and quantum-chemical calculations. The change in the magnetic behavior by replacement of *d*-metal in $La_{21}Fe_8M_7C_{12}$ by Mn, as well as influence of *p*-elements M on the magnetic properties of $La_{21-\delta}Mn_8M_7C_{12}$, is revealed. This sheds new light on the effect of the surrounding La/M network on the magnetic behavior of spin frustrated T_4 clusters in this structure.

EXPERIMENTAL SECTION

Sample Preparation. The synthesis of $La_{21-\delta}Mn_8M_7C_{12}$ (M = Sn, Bi, Sb, Ge, Te) was carried out following the procedure described for $La_{21}Fe_8Sn_7C_{12}$. The starting materials were stored and handled in an argon-filled glovebox. Powders of lanthanum (99.9%, Alfa Aesar), manganese (Alfa Aesar, 99.6%), carbon (95−97%, Strem Chemicals), tin (99.9%, Fisher Chemicals), bismuth (99.9%, Strem Chemicals), antimony (99.5%, Strem Chemicals), tellurium (Ventron Alfa Products, 99.9%), germanium (Alfa Aesar, 99.999%), aluminum (99%, Strem Chemicals), and ingots of La−Ni eutectic (88:12 wt %, Alfa Aesar 99.9%) were used as received. Starting materials La, Mn, C, and M (M = Sn, Bi, Sb. Ge, Te), mixed in 21:8:7:12 molar ratio (total mass 0.43 g), were sandwiched between layers of La/Ni eutectic (~1.4 g, broken into small pieces) with slightly more flux in the top layer compared to the bottom one. Subsequently, to check reproducibility of the synthesis of Te- and Ge-containing compounds and study the possible doping by Al, samples with molar ratios La:Mn:Te:C = 20:8:7:12, La:Mn:Te:Al:C = 20:8:4:3:12, La:Mn:Ge:C = 21:8:7:12, and La:Mn:Ge:Al:C = 21:8:5:2:12 were reacted in La/Ni flux following the same procedure.

For each flux reaction, all the reactants were placed into an alumina crucible (i.d. 6 mm) with a second alumina crucible filled with Fiberfrax and inverted above the reaction crucible to act as a filter during centrifugation. The alumina crucibles were placed into a silica tube, which was fused under a vacuum of 10^{-2} Torr; the ampule was then

Table 2. Atomic Coordinates and Equivalent Displacement Parameters (Å^2) for $La_{21}Mn_8Sn_7C_{12}$ (I), $La_{21}Mn_8Ge_{6.2}Al_{0.8}C_{12}$ (IV), and $La_{20}Mn_8Te_7C_{12}$ (V)

atom	Wyckoff	s.o.f.	*x*/*a*	*y*/*b*	*z*/*c*	U_{eq}[a]
			$La_{21}Mn_8Sn_7C_{12}$			
La(1)	48*h*	1	0	0.1708(1)	*y*	0.012(1)
La(2)	32*f*	1	0.3657(1)	*x*	*x*	0.011(1)
La(3)	4*b*	1	1/2	1/2	1/2	0.021(1)
Mn	32*f*	1	0.1972(1)	*x*	*x*	0.012(1)
Sn(1)	24*e*	1	0.2888(1)	0	0	0.013(1)
Sn(2)	4*a*	1	0	0	0	0.014(1)
C	48*g*	1	0.1078(5)	1/4	1/4	0.015(1)
			$La_{21}Mn_8Ge_{6.17(2)}Al_{0.83(2)}C_{12}$			
La(1)	48*h*	1	0	0.1657(1)	*y*	0.013(1)
La(2)	32*f*	1	0.3691(1)	*x*	*x*	0.011(1)
La(3)	4*b*	1	1/2	1/2	1/2	0.038(1)
Mn	32*f*	1	0.1952(1)	*x*	x	0.012(1)
Ge(1)	24*e*	1	0.2910(1)	0	0	0.013(1)
Ge(2)/Al(2)	4*a*	0.17(2)/0.83	0	0	0	0.018(2)
C	48*g*	1	0.1047(5)	1/4	1/4	0.021(1)
			$La_{20.02(1)}Mn_8Te_7C_{12}$			
La(1)	48*h*	1	0	0.17067(2)	y	0.0094(1)
La(2)	32*f*	1	0.36465(2)	*x*	*x*	0.0090(1)
La(3)	4*b*	0.024(5)	1/2	1/2	1/2	0.0090(1)
Mn	32*f*	1	0.19537(5)	*x*	*x*	0.0082(2)
Te(1)	24*e*	1	0.28578(4)	0	0	0.0111(2)
Te(2)	4*a*	1	0	0	0	0.0335(5)
C	48*g*	1	0.1056(4)	1/4	1/4	0.021(1)

[a] U_{eq} is defined as one-third of the trace of the orthogonalized U_{ij} tensor.

dx.doi.org/10.1021/cm1028595 |*Chem. Mater.* 2011, 23, 1768–1778

Table 3. Selected Interatomic Distances (Å) in the Structures of $La_{21}Mn_8Sn_7C_{12}$ (I), $La_{21}Mn_8Bi_7C_{12}$ (II), $La_{21}Mn_8Sb_7C_{12}$ (III), $La_{21}Mn_8Ge_{6.2}Al_{0.8}C_{12}$ (IV), and $La_{20}Mn_8Te_7C_{12}$ (V)

bond	$La_{21}Mn_8Sn_7C_{12}$	$La_{21}Mn_8Bi_7C_{12}$	$La_{21}Mn_8Sb_7C_{12}$	$La_{21}Mn_8Ge_{6.2}Al_{0.8}C_{12}$	$La_{20}Mn_8Te_7C_{12}$
La−La	3.7484(9)−4.0455(5)	3.7276(8)−4.0077(4)	3.7505(7)−3.9563(2)	3.8011(5)−3.9654(3)	3.6903(8)−3.9692(4)
M(1)−La(1) × 4	3.4764(5)	3.4684(3)	3.4374(3)	3.3709(7)	3.3854(4)
M(1)−La(2) × 4	3.4302(4)	3.4202(3)	3.3758(3)	3.2607(5)	3.4047(4)
M(1)−La(3)	3.5356(8)	3.4701(4)	3.4454(6)	3.391(1)	3.5230(7)
M(2)−La(1) × 12	4.0455(5)	4.0077(4)	3.9523(3)	3.8011(4)	3.9691(3)
Mn−Mn × 3	2.502(3)	2.534(2)	2.515 (2)	2.514(2)	2.541(2)
Mn−C × 3	1.949(7)	1.954(6)	1.951(4)	1.934(7)	1.948(5)
Mn−La(1) × 3	3.360(1)	3.310(1)	3.2900(8)	3.240(1)	3.264(1)
Mn−La(2) × 3	3.1911(5)	3.1191(5)	3.1264(4)	3.1829(5)	3.1142(5)
C−La(1) × 2	2.602(6)	2.569(5)	2.558(4)	2.575(6)	2.534(5)
C−La(2) × 2	2.776(2)	2.717(1)	2.724(1)	2.765(1)	2.711(1)

heated to 950 °C in 3 h, held at this temperature for 12 h, and then cooled to 850 °C in 10 h. The reaction mixtures were subsequently annealed for 48 h at 850 °C and then cooled to 600 °C in 84 h. At 600 °C the ampule was removed from the furnace, quickly inverted, and placed into a centrifuge to decant the molten flux. To separate the crystals from residual La−Ni coating, samples were washed with ethanol and kept in an argon-filled glovebox or stored in a refrigerator under paratone oil to prevent further oxidation.

Elemental Analysis. Semiquantitative elemental analysis was performed with energy-dispersive X-ray spectroscopy (EDXS) on a JEOL 5900 scanning electron microscope equipped with PGT Prism energy dispersion spectroscopy software. Crystals were affixed to an aluminum sample puck with carbon tape, oriented with a flat face perpendicular to the beam, and analyzed using a 30 kV accelerating voltage and an accumulation time of 60 s. The carbon content was not determined due to the limitation of EDXS with light elements. The samples were also monitored for Ni and Al contamination, which may stem from the flux or be leached from the crucible, respectively. No Ni was detected, but small amounts of Al were found for all samples, which might be due to the aluminum sample puck. To test for incorporation of Al all site occupancies were allowed to vary in the single-crystal XRD final refinement cycles (vide infra).

Single Crystal X-ray Diffraction. Selected single crystals were mounted on glass fibers using epoxy. The X-ray intensity data were collected at room temperature on a Bruker SMART APEX2 CCD diffractometer equipped with a Mo-target X-ray tube (λ = 0.71073 Å). The data sets were recorded as ω-scans at 0.3° stepwidth and integrated with the Bruker SAINT software.[10] Data were corrected for absorption effects with either an analytical absorption correction using face-indexing of the crystal or by the multiscan method (SADABS[11]). The structures were solved in the centrosymmertic space group $Fm\bar{3}m$ (No. 225) and refined by full-matrix least-squares procedures on $|F^2|$ using the SHELX-97 software package.[12] The positions of all atoms except for carbon were found by direct methods. The position of carbon was located after a series of least-squares cycles and difference Fourier maps. The occupancy factors for all atomic positions were allowed to vary and found to be close to unity in structures $La_{21}Mn_8Sn_7C_{12}$ (I), $La_{21}Mn_8Bi_7C_{12}$ (II), and $La_{21}Mn_8Sb_7C_{12}$ (III) (Tables 1 and 2 and Supporting Information Table S1). The larger ADP (atomic displacement parameter) in the case of positions La(3) or M(2) can be attributed to the "rattling" of these loosely bonded atoms.[13] The refinement of these positions as split sites with higher multiplicity was found to be unstable.

In the case of $La_{21}Mn_8Ge_{6.2}Al_{0.8}C_{12}$ (IV) (Tables 1 and 2), position 4*a* showed partial occupancy when set solely occupied by germanium. Taking into account that EDXS analysis showed Al incorporation in the case of (IV), this position was refined as mixed occupied by Ge(2)/Al(2). For the structure of $La_{20}Mn_8Te_7C_{12}$ (V) (Tables 1 and 2), the refinement of occupancies showed that position 4*b* is partially occupied by La(3). To exclude high correlations between ADP and sof and in order to estimate the occupancy of this position correctly, the ADP for La(3) was constrained to be equal to that of La(2) and the occupancy of La(3) position was allowed to vary. This results in a 2.4(5)% occupancy of La(3) position for the structure (V). Removing this atom completely from the refinement leads to the appearance of a significant residual electron density peak in the difference Fourier map in the vicinity of the La(3) position.

The final refinement with anisotropic atomic displacement parameters (ADP) for all atoms converged to R_1 = 0.018, 0.019, 0.018, 0.020, and 0.023 leading to the compositions $La_{21}Mn_8Sn_7C_{12}$ (I), $La_{21}Mn_8Bi_7C_{12}$ (II), $La_{21}Mn_8Sb_7C_{12}$ (III), $La_{21}Mn_8Ge_{6.17(2)}Al_{0.83(2)}C_{12}$ (IV), and $La_{20.02(1)}Mn_8Te_7C_{12}$ (V), respectively. The details of the data collections and refinements are summarized in Table 1, the atomic parameters are given in Table 2 and Supporting Information Table S1, and selected bond distances are listed in Table 3.

Magnetic Properties. Magnetic susceptibility data for $La_{21-\delta}Mn_8E_7C_{12}$ (M = Sn, Bi, Sb, Ge/Al, Te) were measured over the temperature range 1.8−300 K using a SQUID magnetometer (Quantum Design MPMS system). Several single crystals (2−30 mg each) were sealed into kapton tape and inserted into a plastic straw. Field-cooled (FC) and zero-field-cooled (ZFC) measurements were performed at various fields, while field-dependent measurements were done at 1.8 K. AC-susceptibility data were collected from 1.8 to 15 K with an applied AC-field of 5 Oe at four different frequencies.

Computational Details. Calculations of density of states (DOS) were performed utilizing the tight binding−linear muffin tin orbitals−atomic sphere approximation TB-LMTO-ASA program package.[14] For the calculations of DOS of $La_{21}Mn_8Sn_7C_{12}$, $La_{21}Mn_8Sb_7C_{12}$, $La_{21}Mn_8Bi_7C_{12}$, and $La_{20}Mn_8Te_7C_{12}$ the experimental room-temperature structural parameters (unit cell dimensions, space group, and atomic coordinates) were used, while for the DOS of hypothetical $La_{21}Mn_8Te_7C_{12}$ the structural parameters of $La_{20}Mn_8Te_7C_{12}$ with addition of the fully occupied La(3) site were employed. The radial scalar-relativistic Dirac equation was solved to obtain the partial waves. The calculation was made for 145 k-points in the irreducible Brillouin zone. Integration over the Brillouin zone was made by the tetrahedron method.[15] The basis set contained La (6s, 5d, 4f), Mn (4s, 4p, 3d), Sn/Sb/Te (5s, 5p), Bi (6s, 6p), and C (2s, 2p) with La(6p), Sn/Sb/Te(5d, 4f), Bi(6d, 5f), and C(3d) functions being downfolded. The radii of atomic spheres used for the calculations are listed in the footnote.[16] Interstitial empty spheres (0.61 Å ≤ r(E) ≤ 0.90 Å) were added to fill the interstitial space.

dx.doi.org/10.1021/cm1028595 |*Chem. Mater.* 2011, 23, 1768–1778

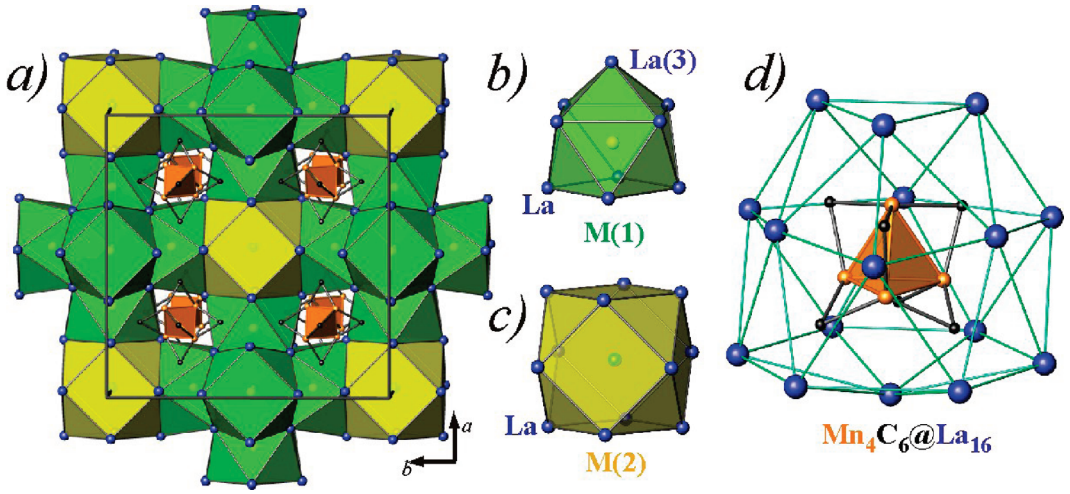

Figure 1. (a) Polyhedral representation of the crystal structure of $La_{21-\delta}Mn_8M_7C_{12}$ (M = Ge/Al, Sn, Sb, Te, Bi) in *ab*-plane; coordination polyhedra of M(1) (green) and M(2) (yellow) by La atoms are emphasized. La atoms are drawn in blue, Mn atoms in orange, and C atoms in black. (b) Coordination polyhedron for M(1) site (monocapped square antiprism) by La atoms. (c) Coordination polyhedron of M(2) site (cuboctahedron) by La atoms. (d) The 16-vertex Frank-Kasper polyhedral cage of La atoms around the Mn_4C_6 cluster.

Mössbauer Spectroscopy. A $^{57}Co/Rh$ and a $Ca^{119m}SnO_3$ source were available for the ^{57}Fe and ^{119}Sn Mössbauer spectroscopic investigations, respectively. The samples were placed within thin-walled plexiglass containers at a thickness of about 10 mg Sn(Fe)/cm^2. In the case of the ^{119}Sn measurements a palladium foil of 0.05 mm thickness was used to reduce the tin K X-rays concurrently emitted by this source. The measurements were conducted in the usual transmission geometry at 4.2, 77, and 298 K.

RESULTS AND DISCUSSION

Synthesis. $La_{21-\delta}Mn_8M_7C_{12}$ (M = Sn, Sb, Bi, Te, Ge/Al) phases were synthesized by flux growth from La/Ni eutectic according to the procedure described for Fe analogues $La_{21}Fe_8M_7C_{12}$.[6] The La/Ni eutectic mixture readily dissolves carbon and transition metals and allows the growth of relatively large crystals of complex intermetallics. The cubic phases $La_{21-\delta}Mn_8M_7C_{12}$ (M = Sn, Sb, Bi, Te, Ge/Al) crystallize as silver, reflective, well-faceted crystals having the form of truncated cubes of up to 1 mm on a side or crystal agglomerates (Supporting Information Figure S1). Despite the significant yield of crystals of the cubic phase $La_{21-\delta}Mn_8M_7C_{12}$ (up to 30%), the samples also contain well-crystallized specimens of other phases, but in considerably smaller amounts. These byproducts could be easily distinguished from the $La_{21-\delta}Mn_8M_7C_{12}$ phase based on different crystal habits, color, EDX analysis, and screening of the crystals on the X-ray single crystal diffractometer. In the case of M=Sb and Bi the byproduct was found to be carbide $La_{3.67}MnC_6$.[17,18] The sample of $La_{21}Mn_8Sn_7C_{12}$ contains crystals of a new quaternary carbide $La_{14}SnMn_3C_{18}$ with crystal structure closely related to that of $La_{3.67}MnC_6$.[18]

In the case of M = Te the formation of $La_{20}Mn_8Te_7C_{12}$, where one of the lanthanum positions is almost vacant (vide infra), was proved to be reproducible, since the refinement of the crystal structure of several crystals selected from two different samples with starting composition La:Mn:Te:C = 21:8:7:12 or 20:8:7:12 gives the same result. The byproduct crystals of these reactions include $La_{3.67}MnC_6$ and La_2O_2Te phases.[19] The lanthanum oxytelluride La_2O_2Te (*anti*-$ThCr_2Si_2$ structure type) was previously reported to form from reaction of lanthanum oxide and tellurium in hydrogen flow[19a] or from reaction of lanthanum metal and tellurium dioxide.[19b] The strong reducing nature of La/Ni eutectic leaches oxide from the alumina crucible used in the synthesis and leads to in situ formation of lanthanum oxide. Lanthanum oxide subsequently dissolves in La/Ni eutectic and reacts with tellurium to form La_2O_2Te crystals. Since the Te analogue with T = Fe consistently incorporated Al (forming $La_{21}Fe_8Te_4Al_3C_{12}$), this was also explored for the T = Mn reactions with deliberate addition of aluminum with the starting composition $La_{21}Mn_8Te_4Al_3C_{12}$ (similar to the Fe analogue[6]). However, this did not lead to the cubic phase. Instead, crystals of $La_{3.67}MnC_6$, La_2O_2Te and $LaMn_{2-x}Al_x$ (Cu_2Mg-structure type) phases formed.

From the refinement of the single-crystal data for the M = Ge analogue (vide infra), aluminum was shown to incorporate into one of the sites in the structure. In the first set of syntheses aluminum was not added deliberately but was leached from the alumina crucible and incorporated into the crystal structure of $La_{21}Mn_8Ge_{6.2}Al_{0.8}C_{12}$. The incorporation of aluminum was shown to be reproducible for this analogue; refinement of the crystal structure for several crystals selected from two batches prepared separately but with the same starting composition La:Mn:Ge:C = 21:8:7:12 gives the same Ge/Al ratio within accuracy of determination. The Al incorporation limit was studied by preparation of the sample with aluminum deliberately added. However, crystals selected from the sample with starting composition La:Mn:Ge:Al:C = 21:8:5:2:12 have the same Ge/Al ratio. Thus, the incorporation of a specific amount of aluminum might be necessary to stabilize $La_{21}Mn_8M_7C_{12}$ in the case of M = Ge; the preferred Ge/Al ratio was found to be 6.2/0.8.

Crystal Structure. $La_{21}Mn_8M_7C_{12}$ (M = Sn, Sb, Bi) is isostructural to $La_{21}Fe_8M_7C_{12}$ and features isolated manganese tetrahedra edge-capped by carbon atoms (Figure 1). There are eight Mn_4C_6 clusters in the *F*-centered cubic unit cell, which are isolated from each other and embedded in the La/M (M = Sn, Bi, Sb, Te, Ge/Al) network. The M atoms have two distinct environments. The M(1) site is surrounded by nine La atoms and is found in the center of a monocapped square antiprism, M(1)@La_9. The M(2) site in the origin of the unit cell is

dx.doi.org/10.1021/cm1028595 |*Chem. Mater.* 2011, 23, 1768–1778

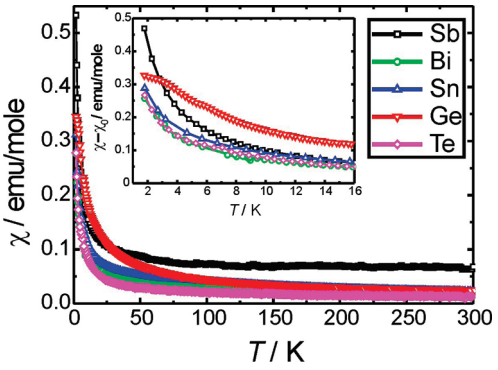

Figure 2. Temperature dependence of field-cooled magnetic susceptibility, $\chi(T)$, collected at applied field of H = 100 Oe for $La_{21-\delta}Mn_8M_7C_{12}$ (M = Ge/Al, Sn, Sb, Te, Bi) analogues. Inset: low-temperature part of $\chi - \chi_0$ vs T.

coordinated by 12 La atoms at a long distance of ~4 Å in a cubooctahedral fashion, M(2)@La_{12}. Six M(1)-centered antiprisms are linked with each other by sharing the capping La site. Each of the antiprisms has a common square face with the cuboctahedron centered by M(2). Thus, cuboctahedrons M(2)@La_{12} are isolated from each other but are connected with antiprisms M(1)@La_9 forming an extended three-dimensional La/M network with channels accommodating Mn_4C_6 clusters, as shown in Figure 1. Each Mn_4C_6 cluster is surrounded by lanthanum atoms forming a 16-vertex Frank-Kasper polyhedron (tetracapped truncated tetrahedron with caps on the four hexagonal faces). Within the ideal nondistorted Mn_4-tetrahedra the distance between Mn atoms is ~2.52 Å, which is comparable with the homoatomic distance in α- and β-Mn (2.26−2.63 Å) and $TiMnSi_2$,[20] UMn_5Al_7,[21] $Zr_3Mn_4Si_6$,[22] Er_2MnC_4,[23] and $Gd_3Mn_2C_6$.[24] The Mn−C distance of 1.95 Å lies in the range seen for other carbides of manganese and rare-earth metals (1.987 Å for Er_2MnC_4,[23] 1.843 Å and 2.143 Å for $Gd_3Mn_2C_6$,[24] and 1.784 Å, 1.824 Å, and 1.943 Å for $Dy_{12}Mn_5C_{15}$ [25]).

Deviations from the ideal La/M framework are seen for two analogues: aluminum incorporation in $La_{21}Mn_8Ge_{6.2}Al_{0.8}C_{12}$ and partial La occupancy in $La_{20.02(1)}Mn_8Te_7C_{12}$. In the case of $La_{21}Mn_8Ge_{6.2}Al_{0.8}C_{12}$, incorporation of aluminum into the M(2) site is evident from the refinement of single-crystal X-ray data (83% Al). Similar behavior was seen for the Fe analogue, $La_{21}Fe_8Ge_{4.9}Al_{2.1}C_{12}$, where Al atoms mainly occupy the M(2) position (84% of Al in M(2) site) but are also present in the M(1) position (20.3%). The similar sizes of aluminum and germanium may promote the incorporation of aluminum into the M = Ge analogues for both the iron and manganese phases. For the tellurium-containing compound $La_{20.02(1)}Mn_8Te_7C_{12}$, the occupancy of the lanthanum capping site, La(3), is only around ~2%; therefore, the coordination polyhedron of Te(1) is not a monocapped square antiprism as for other analogues $La_{21-\delta}Mn_8M_7C_{12}$ (M = Ge/Al, Sn, Sb, Bi) but rather a square antiprism with CN(Te(1)) = 8. The partial occupancy of the La(3) position was also observed in a reinvestigation of the structure of the iron analogue $La_{20.71(4)}Fe_8Te_{4.34(9)}Al_{2.66(9)}C_{12}$,[26] where the occupancy of capping the La(3) site is 69%. However, for the iron analogue, incorporation of aluminum into the M(1) site is observed, which is not the case for Mn analogue $La_{20}Mn_8Te_7C_{12}$. Apparently, vacancy formation in one of the lanthanum positions is needed to stabilize $La_{21-\delta}T_8Te_7C_{12}$ (T = Fe or Mn); this is supported by electronic calculations (vide infra).

Table 4. Fitting Parameters of FC Magnetic Susceptibility, χ, Collected at Applied Field of H = 100 Oe with Modified Curie-Weiss Law, $\chi = \chi_0 + C/(T - \theta)$, for the Different Analogues of $La_{21-\delta}Mn_8M_7C_{12}$ (M = Ge/Al, Sn, Sb, Te, Bi)[a]

	Ge/Al	Sn	Sb	Te	Bi
χ_0, emu/mol	0.0134(2)	0.0238(4)	0.0634(1)	0.01116(1)	0.0199(1)
θ, K	−10(2)	−3.0(1)	−0.44(2)	−1.62(3)	−1.79(5)
C	3.46(8)	1.26(3)	1.033(5)	0.865(6)	0.871(8)
μ_{eff} per Mn atom, μ_B	1.87	1.13	1.02	0.93	0.94

[a] The fitting for compounds with M = Sn, Sb, Te, and Bi was done in the temperature range of 1.8−300 K; for the analogue with M = Ge/Al the fitting was done for $T \geq 100$ K.

The replacement of Fe with Mn in $La_{21-\delta}T_8Te_7C_{12}$ leads to the concomitant increase of the size of the cubic unit cell, which is in line with the larger atomic radius of Mn compared to Fe (Supporting Information Figure S2). Moreover, the change in the M element (M = Ge/Al, Sn, Sb, Bi, Te) leads to identical trends in the unit cell parameter for both Mn and Fe analogues. The cubic unit cell parameter, a, changes as follows: $a_{Sn} > a_{Bi} > a_{Sb} > a_{Te} > a_{Ge}$ reflecting the trend of atomic radius increasing going down a Group and decreasing from left to right along a Period (Supporting Information Figure S2). The compression of the unit cell is mainly associated with the change in M−La distances (Supporting Information Figure S3); Mn−Mn and Mn−C distances are less affected (Table 3).

Magnetic Properties. The FC (field-cooled) magnetic susceptibility vs T data for $La_{21-\delta}Mn_8M_7C_{12}$ (M = Ge/Al, Sn, Sb, Te, Bi) are shown in Figure 2. The compounds with M = Sn, Sb, Te, Bi and are paramagnetic; data for the analogue with M = Ge/Al have curvature not typical for a simple paramagnet at low temperatures ($T \leq 100$ K). The $\chi(T)$ plots were fitted with the modified Curie−Weiss law: $\chi = \chi_0 + C/(T - \theta)$ (Table 4), where C is the Curie constant, $C = N\mu^2_{eff}/3\kappa_B$, θ is the Weiss constant (or paramagnetic Curie temperature), and χ_0 is a temperature-independent term which includes the contributions from Pauli and Van Vleck paramagnetism as well as core and Landau diamagnetism. The fits were done in the temperature range of 1.8−300 K for all analogues except for $La_{21}Mn_8Ge_{6.2}Al_{0.8}C_{12}$: for the latter, the fit was done at temperatures above 100 K, well above the magnetic transition.

The relatively large and positive temperature-independent contribution to $\chi(T)$ observed for all phases is indicative of Pauli paramagnetism due to conduction electrons and may also partially stem from traces of impurities such as residual flux coating. The observed Pauli paramagnetism is typical for metals and this is in agreement with the calculated density of states (vide infra). The effective paramagnetic moment per Mn atom, μ_{eff}, derived from the Curie constant, C, and assuming that all Mn atoms are magnetically equal is around ~1 μ_B for all analogues, except for $La_{21}Mn_8Ge_{6.2}Al_{0.8}C_{12}$. Similar values for Mn magnetic moments are seen in other Mn-containing intermetallics; these magnetic moments are much lower than the values commonly seen for ionic manganese compounds (4.9 μ_B for Mn^{3+} and 5.9 μ_B for Mn^{2+}).[27] The Weiss constant, θ, shows the strength and type of coupling between neighboring magnetic centers and is usually similar in magnitude to the ordering temperature. For $La_{21-\delta}Mn_8M_7C_{12}$ (M = Sn, Sb, Te, Bi) the Weiss constant is negative and its value is very small, which implies rather weak antiferromagnetic (AFM) exchange interactions between Mn

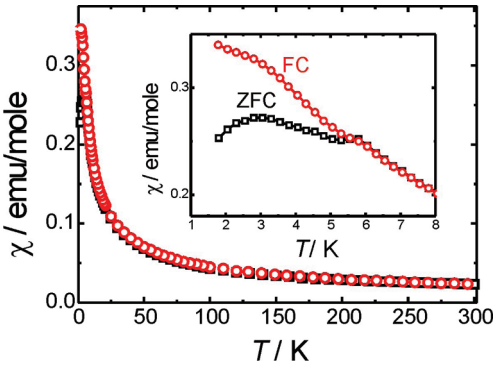

Figure 3. ZFC-FC magnetic susceptibility, $\chi(T)$, collected at applied field of H = 100 Oe for $La_{21}Mn_8Ge_{6.2}Al_{0.8}C_{12}$. Inset: low-temperature part of $\chi(T)$ shows ZFC-FC divergence.

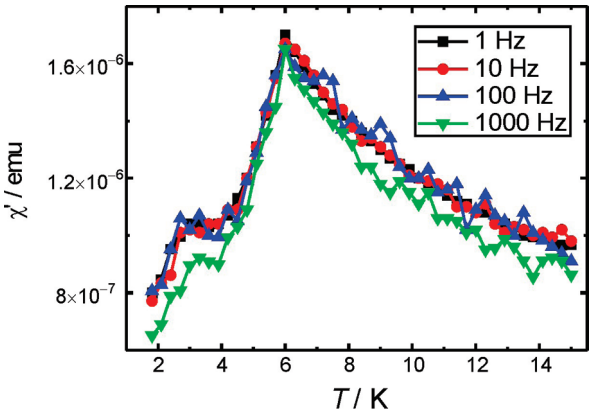

Figure 4. Temperature dependence of the real component of AC-susceptibility, χ', for $La_{21}Mn_8Ge_{6.2}Al_{0.8}C_{12}$ at different frequencies.

atoms. This contrasts with the much larger magnitude of the Weiss constant in the case of the iron analogue, $La_{21}Fe_8Sn_7C_{12}$, which indicates stronger AF exchange between Fe moments compared to Mn. The dependence of the product of χT vs T for $La_{21-\delta}Mn_8M_7C_{12}$ (M = Sn, Sb, Te, Bi, Ge) (Supporting Information Figure S4) can be separated into two contributions: linear decrease of χT with decreasing temperature, which is due to the temperature-independent part of the susceptibility, and further negative deviations from this linear decrease at $T \leq 100$ K, which is a result of AFM coupling between magnetic centers. In the case of M = Sb the temperature-independent term is dominant and magnetic coupling is negligible. For the analogues with M = Te or Bi the AFM coupling is also rather small, while for M = Sn the coupling is larger. From the dependence of χT vs T substantial AFM interactions between Mn atoms are apparent for the analogue with M = Ge. This enhancement of AFM coupling between Mn centers in $La_{21-\delta}Mn_8M_7C_{12}$ with changing of M in the order Sb → Te → Bi → Sn → Ge is also reflected in the change of Weiss constant values (Table 4). The compound $La_{21}Mn_8Ge_{6.2}Al_{0.8}C_{12}$ is characterized by the strongest AFM coupling between Mn atoms (largest magnitude of θ), highest moment per Mn atom and deviations in $\chi(T)$ from simple paramagnetic behavior at low temperatures; therefore, additional measurements were performed on this phase.

ZFC-FC magnetic susceptibility data sets for $La_{21}Mn_8Ge_{6.2}Al_{0.8}C_{12}$ collected at a field of H = 100 Oe exhibit splitting at $T_1 \approx 6$ K, suggesting a significant irreversibility in the alignment of magnetic moments (Figure 3). An additional cusp in the ZFC susceptibility and change of slope for FC susceptibility are seen at $T_2 \approx 3$ K. Such behavior was found to be reproducible for crystals of $La_{21}Mn_8Ge_{6.2}Al_{0.8}C_{12}$ selected from several samples. The feature at 6 K is suppressed at applied field above 0.1 T, which results in disappearance of the ZFC-FC divergence, while the change of slope at 3 K remained even at higher field (up to 1 T) (Supporting Information Figure S5). The magnetization measured at 1.8 K as a function of field, $M(H)$, does not saturate up to the highest available field of 7 T and exhibits a positive curvature with increasing field. The hysteresis is found to be negligible (less than 0.005 T) (Supporting Information Figure S6).

A spin glass state is usually indicated by ZFC-FC splitting at T_{SG} together with a frequency dependence of the real part of ac-susceptibility, χ', and a Mydosh parameter, φ, in the range of 0.004−0.08, where $\varphi = \Delta T_{SG}/[T_{SG} \log \omega]$ (T_{SG} is the temperature of the cusp, ω is frequency).[28] The Sn-containing iron analogue $La_{21}Fe_8Sn_7C_{12}$ exhibits clear spin-glass behavior with T_{SG} = 5 K.[6] Since $La_{21}Mn_8Ge_{6.2}Al_{0.8}C_{12}$ also exhibits ZFC-FC divergence which might be indicative of spin-glassiness, AC-susceptibility measurements were performed (Figure 4). The real part of the AC-susceptibility, χ', exhibits cusps at 3 and 6 K in agreement with the dc-susceptibility data. However, no frequency dependence is observed for either transition in $La_{21}Mn_8Ge_{6.2}Al_{0.8}C_{12}$, unlike the behavior seen for $La_{21}Fe_8Sn_7C_{12}$. The observed phenomena at $T_1 \approx 6$ K and $T_2 \approx 3$ K could be attributed to the frustration of the antiferromagnetically coupled magnetic moments within ideal Mn_4 tetrahedra. However, the weaker coupling within and between the Mn_4 tetrahedra in $La_{21}Mn_8Ge_{6.2}Al_{0.8}C_{12}$ cannot produce the cooperative freezing transition of a spin-glass such as that seen in the more strongly coupled $La_{21}Fe_8Sn_7C_{12}$. Among all the Mn analogues, only $La_{21}Mn_8Ge_{6.2}Al_{0.8}C_{12}$ features mixed occupation of the M(2) site by Ge/Al. The associated disorder in the M(2) site may cause perturbations of the lanthanum network and thus may influence the local environment of the Mn_4C_6 cluster (Figure 1c), possibly leading to slight distortions. This will lower the local symmetry of the Mn_4 tetrahedral unit and thereby induce different exchange interactions between neighboring manganese atoms, eliminating frustration and leading to the appearance of two features in $\chi(T)$ at different temperatures.

Electronic Structure. The $La_{21}T_8M_7C_{12}$ structure is stable for two 3*d*-transition metals, T = Fe or Mn, and for a number of M elements of groups 14−16, namely, M = Sn, Bi, Sb, Te/Al, and Ge/Al. The valence electron count (VEC) varies with the M and T elements, so a straightforward correlation between the stability of the $La_{21}T_8M_7C_{12}$ analogues and VEC is not obvious. For instance, the VEC for $La_{20}Mn_8Te_7C_{12}$ is 206, but $La_{21}Mn_8Te_7C_{12}$ with VEC of 209 does not exist, even though VEC for the existing Fe analogue $La_{21}Fe_8Bi_7C_{12}$ is 210. For more insight, electronic structure calculations were performed with the TB-LMTO-ASA program for the four analogues: $La_{21}Mn_8Sn_7C_{12}$, $La_{21}Mn_8Sb_7C_{12}$, $La_{21}Mn_8Bi_7C_{12}$, $La_{20}Mn_8Te_7C_{12}$, and a hypothetical "$La_{21}Mn_8Te_7C_{12}$". These four compounds are paramagnetic; therefore, nonspin-polarized calculations were carried out. The hypothetical "$La_{21}Mn_8Te_7C_{12}$", with a fully occupied La(3) site, was studied for comparison to the experimentally found composition $La_{20}Mn_8Te_7C_{12}$, where the La(3) site is essentially vacant.

The density-of-states (DOS) plots for $La_{21}Mn_8Sn_7C_{12}$, $La_{21}Mn_8Sb_7C_{12}$, and hypothetical "$La_{21}Mn_8Te_7C_{12}$" are presented

dx.doi.org/10.1021/cm1028595 |*Chem. Mater.* 2011, 23, 1768–1778

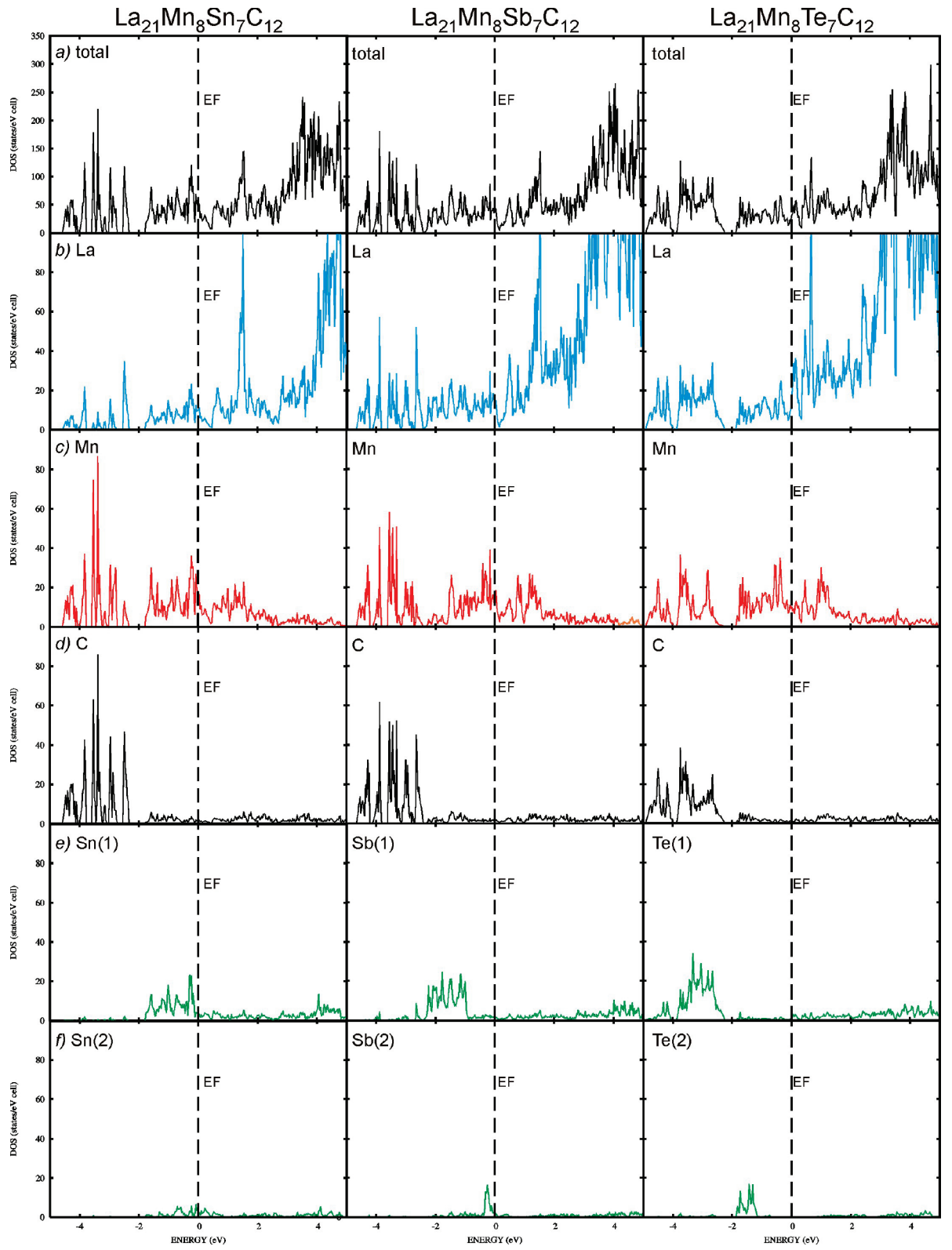

Figure 5. Total (a) and partial (b−f) density-of-states plots for $La_{20}Mn_8Sn_7C_{12}$, $La_{20}Mn_8Sb_7C_{12}$, and hypothetical "$La_{21}Mn_8Te_7C_{12}$". Note the different scale of the *y*-axis for (a) and (b−f) while the scale for the *x*-axis is the same.

in Figure 5. The DOS plot for $La_{21}Mn_8Bi_7C_{12}$ (Supporting Information Figure S7) is similar to that of the Sb analogue. The nonzero DOS at the Fermi level indicates that all the compounds are metallic. Notably, the *d*-states of lanthanum contribute significantly to the states near and below the Fermi level, which indicates that the simple view of charge distribution, with lanthanum considered as a La^{3+} ion, is not necessarily applicable for this lanthanum-rich intermetallic. The states in the valence

dx.doi.org/10.1021/cm1028595 |*Chem. Mater.* 2011, 23, 1768–1778

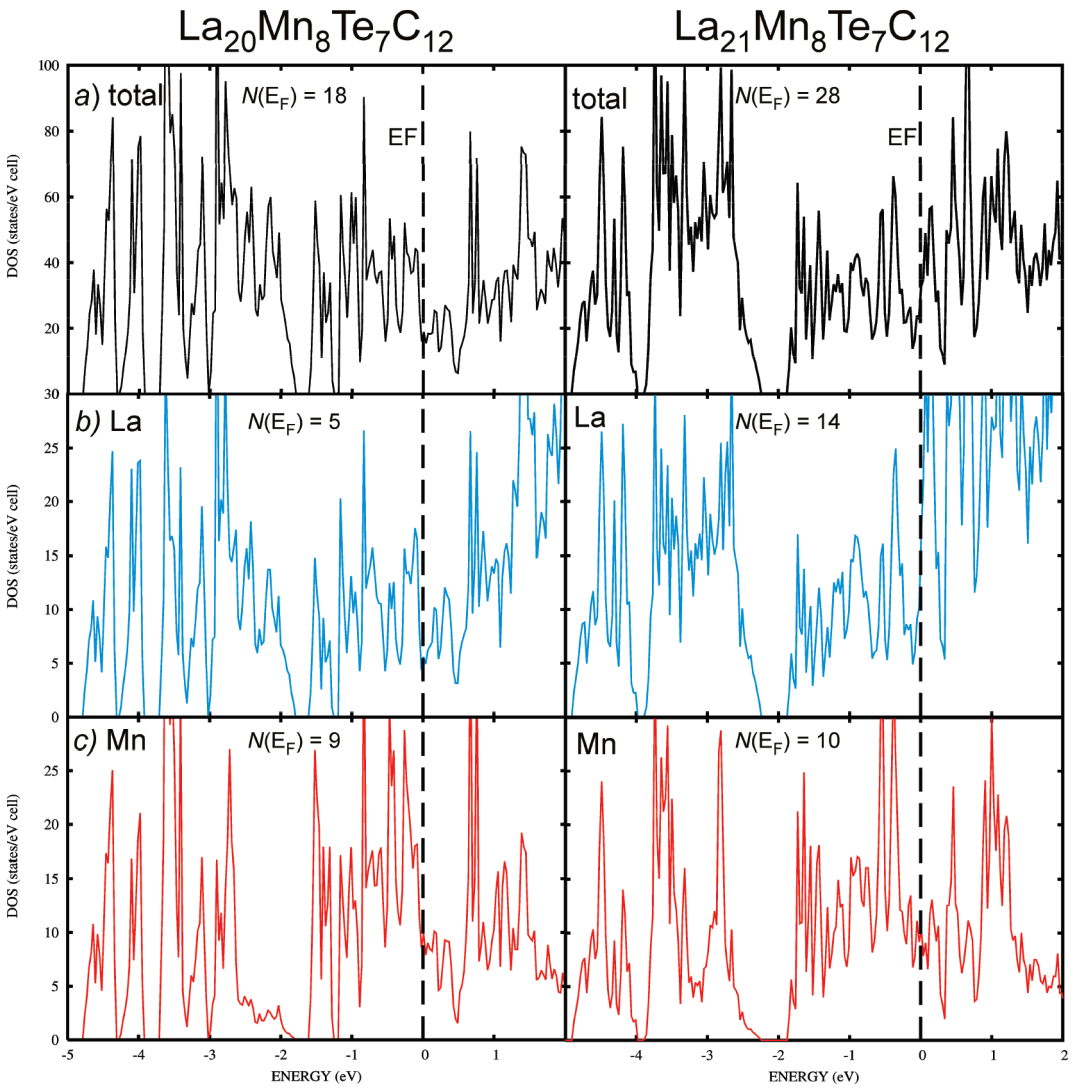

Figure 6. Total (a) and partial (b, c) density-of-states plots for $La_{20}Mn_8Te_7C_{12}$ and hypothetical "$La_{21}Mn_8Te_7C_{12}$". Note the different scale of *y*-axis for (a) and (b, c) while the scale for the *x*-axis is the same.

region between −5 and 0 eV are composed of the *p*-states of C and M and *d*-states of both Mn and La with minor contributions from Mn-*s*, Mn-*p*, La-*s*, and La-*f* states.

The DOS for $La_{21}Mn_8M_7C_{12}$, where M are elements of the same period (M = Sn, Sb, Te), are very similar; the main difference is in the location of *p*-orbitals of M elements (Figure 5). For M = Sn the *p*-states contribute to the levels at the Fermi level, while for M = Te these states are located well below the Fermi level. This situation reflects that the *p*-orbitals in the case of the more electronegative M = Te are more localized compared to M = Sn, supporting the assumption about the decrease of ionic contribution in La−M interactions along the row Te → Sb → Sn. This shift of the M *p*-states results in rearrangement of the electronic structure of $La_{21}Mn_8M_7C_{12}$ leading to the decrease of the La states contribution to the states at the Fermi level along the row Te → Sb → Sn (from 15.3 states/eV cell for M = Te to 9.7 states/eV cell for M = Sn), while the contribution of Mn shows the opposite trend (from 10.3 states/eV cell for M = Te to 16.4 states/eV cell for M = Sn).

The DOS of $La_{20}Mn_8Te_7C_{12}$ and hypothetical "$La_{21}Mn_8Te_7C_{12}$" are very similar. However, in the case of the hypothetical vacancy-free composition, the DOS exhibits a significant peak at the Fermi level, which is in general considered a sign of instability. This peak is mainly derived from La-*d* states as can be seen in Figure 6b and Supporting Information Figure S8 ($N_{La}(E_F)$ = 14 states/eV cell). In the DOS of the experimentally

Table 5. Fitting Parameters of ^{57}Fe and ^{119}Sn Mössbauer Spectra of $La_{21}Fe_8Sn_7C_{12}$ and $La_{21}Mn_8Sn_7C_{12}$[a]

compound	source	*T*, K	δ, mm·s^{-1}	Γ, mm·s^{-1}	ΔE_Q, mm·s^{-1}
$La_{21}Fe_8Sn_7C_{12}$	^{57}Fe	77	−0.13(1)	0.32(1)	0.54(1)
		298	−0.23(1)	0.35(1)	0.54(1)
	^{119}Sn	4.2	2.02(2)	1.58(6)	0.0[b]
		77	2.02(2)	1.21(1)	0.0[b]
		298	1.93(1)	1.07(2)	0.0[b]
$La_{21}Fe_8Sn_7C_{12}$	^{119}Sn	4.2	2.04(1)	1.15(2)	0.0[b]
		77	2.00(1)	1.11(2)	0.0[b]
		298	1.96(1)	1.03(2)	0.0[b]

[a] δ, isomer shift; Γ, experimental line width; ΔE_Q, electric quadrupole splitting parameter. Numbers in parentheses represent the statistical errors in the last digit. [b] Fixed during the fitting procedure.

dx.doi.org/10.1021/cm1028595 |*Chem. Mater.* 2011, 23, 1768–1778

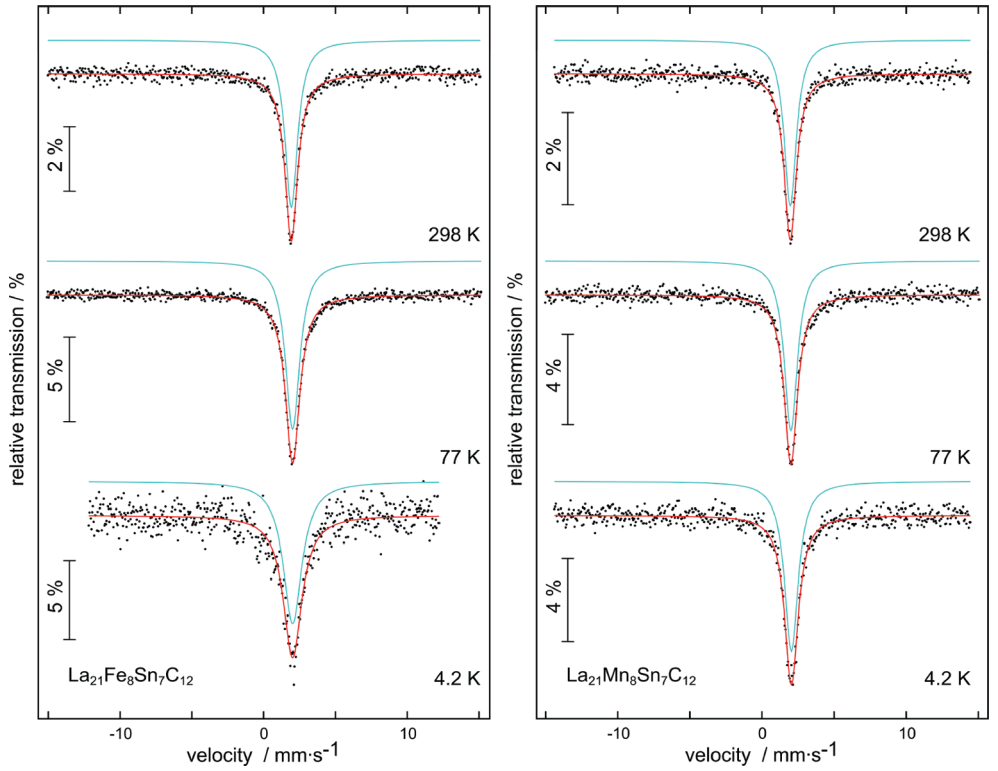

Figure 7. Experimental and simulated ^{119}Sn Mössbauer spectra of $La_{21}Fe_8Sn_7C_{12}$ (left) and $La_{21}Mn_8Sn_7C_{12}$ (right) at 298, 77, and 4.2 K.

observed composition $La_{20}Mn_8Te_7C_{12}$ this instability is removed mainly due to the decrease of La contribution to the states at the Fermi level ($N_{La}(E_F)$ = 5 states/eV cell). Notably, the contribution of Mn states to the states at the Fermi level for both compositions is similar. Thus, the removal of one La atom leads to the lowering of the DOS instability at the Fermi level, and this is likely the reason for the experimentally observed formation of $La_{20}Mn_8Te_7C_{12}$, where La(3) is almost vacant, instead of $La_{21}Mn_8Te_7C_{12}$, where all lanthanum sites would be fully occupied.

Mössbauer Spectroscopy. The isostructural Sn-containing $La_{21}Fe_8Sn_7C_{12}$ and $La_{21}Mn_8Sn_7C_{12}$ compounds were characterized by ^{119}Sn Mössbauer spectroscopy, and $La_{21}Fe_8Sn_7C_{12}$ was additionally characterized by ^{57}Fe Mössbauer spectroscopy. The corresponding fitting parameters are listed in Table 5. The ^{57}Fe Mössbauer spectra of spin-glass compound $La_{21}Fe_8Sn_7C_{12}$ (T_{SG} = 5 K)[6] at 77 and 298 K are presented in Supporting Information Figures S9 together with transmission integral fits. In agreement with the single iron site 32*f*,[6] we observe only one signal at an isomer shift of −0.13 mm/s (77 K data) with quadrupole splitting of 0.54 mm/s. This is a consequence of the low site symmetry and nonsymmetric coordination of iron by three C, three Fe, and additionally six La atoms. The slight increase of the isomer shift from 298 K (−0.23 mm/s) to 77 K can be viewed as a second order Doppler shift (SODS). A negative isomer shift for iron is indicative of a tetravalent iron in the case of oxide compounds and inorganic complexes with large charge transfer. However, in intermetallic compounds with complex electronic structures, the negative isomer shifts cannot be directly correlated with high iron oxidation states.[29] Most likely, the negative shift of Fe is caused by clustering of iron atoms as well as by their surrounding environment of electropositive La atoms. The uniqueness of the $La_{21}Fe_8Sn_7C_{12}$ crystal structure and lack of ^{57}Fe Mössbauer data for similar compounds make comparison rather difficult. Unfortunately, the data at 4.2 K (below the spin glass transition) was too noisy to be fitted; this may be a consequence of the distribution of hyperfine splittings in the disordered spin glass state. A similar phenomenon in spin glasses $FeAl_2$ and $Zn_{77}Fe_7Sc_{16}$ causes extensive broadening of the ^{57}Fe Mössbauer data below the spin glass transition of these compounds.[30]

The ^{119}Sn spectra of $La_{21}Fe_8Sn_7C_{12}$ and $La_{21}Mn_8Sn_7C_{12}$ at 4.2, 77, and 298 K are shown in Figure 7. Although the structures contain two crystallographically independent tin sites, that is, Sn(1) in the 24*e* position (site symmetry 4*mm*) within a cuboctahedron and Sn(2) in the 4*a* position (site symmetry $m\bar{3}m$) within a monocapped square antiprism, all six spectra could be reproduced with a single signal. Most likely the electronic environments of the two tin sites, both surrounded by electropositive La atoms, are very similar, leading to comparable isomer shifts. Consequently we observe an overlap of both signals. This is reflected by the slightly increased experimental line widths. The tin isomer shifts at 77 K of 2.02 mm/s ($La_{21}Fe_8Sn_7C_{12}$) and 2.00 mm/s ($La_{21}Mn_8Sn_7C_{12}$) are typical for intermetallic stannides. Usually in such stannides the isomer shifts range between 1.6 and 2.2 mm/s, for instance $CeRhSn_2$ (2.01 mm/s)[31a] and $CaRhSn_2$ (1.96 mm/s).[31b] Notably, the $La_6Co_{13}Sn$ compound, where isolated Sn atoms reside in the center of bicapped Archimedean antiprisms formed by 10 La atoms, exhibits an isomer shift of 1.94 mm/s at 4.2 K.[32] Consequently, we can assume a substantial *s* electron density at the tin nuclei in $La_{21}Fe_8Sn_7C_{12}$ and $La_{21}Mn_8Sn_7C_{12}$. This situation is in accordance with the systematic isomer shift studies by Lippens,[33] for tin compounds ranging from tin halides, chalcogenides, and pnictides to metallic tin to more anionic tin in Mg_2Sn; it also nicely parallels the electronic structure calculations, where a decrease of the ionic contribution in the

dx.doi.org/10.1021/cm1028595 |*Chem. Mater.* 2011, 23, 1768–1778

La−M interactions is observed in the sequence Te → Sb → Sn (vide ultra).

Comparison of ^{119}Sn spectra at 4.2 K for the spin-glass $La_{21}Fe_8Sn_7C_{12}$ (T_{SG} = 5 K) and the paramagnetic $La_{21}Mn_8Sn_7C_{12}$ reveals significant line broadening in the case of the iron analogue. This might indicate the presence of a distribution of weak transferred hyperfine fields from frozen Fe spins, thus supporting the spin-glass behavior in the case of the $La_{21}Fe_8Sn_7C_{12}$ compound.

CONCLUSION

Reactions of Mn, C, and M in La/Ni eutectic flux result in formation of the carbide phase $La_{21-\delta}Mn_8M_7C_{12}$ (M = Ge/Al, Sn, Sb, Te, Bi), isostructural to the previously reported $La_{21}Fe_8M_7C_{12}$.[6] The La/M network is fairly flexible and adapts to the change of the M element with both mixed occupancy (M/Al) and La vacancies being observed. The analysis of DOS shows evolution of electronic structure with changing of M in $La_{21-\delta}Mn_8M_7C_{12}$ (M = Sn, Sb, Te) and also indicates the necessity of vacancy formation in the case of the Te-containing compound. The nature of the 3*d*-metal has a strong influence on the magnetic properties of $La_{21-\delta}T_8M_7C_{12}$ (T = Fe or Mn). The replacement of Fe with Mn leads to change of the magnetic properties from spin-glassiness for T = Fe and M = Sn to spin-frustration behavior for T = Mn and M = Ge/Al. The frustration is mitigated by the weak coupling between the Mn atoms and local distortions of the Mn_4 tetrahedron caused by the Ge/Al disorder. The magnetic properties of these carbide phases $La_{21-\delta}T_8M_7C_{12}$ (T = Fe or Mn) are governed by magnetic interactions solely between 3*d*-metals, since the La/M network is nonmagnetic. However, the flexibility of the La/M network and its influence on the T_4 coupling introduces avenues to control the nature of the spin-frustration in the tetrahedral T_4 unit. The substitution of nonmagnetic La by other lanthanides with a partially filled *f*-shell (e.g., Ce, Pr, Nd, etc.) may result in even more complex magnetic phenomena originating from interaction of 3*d*- and 4*f*-magnetic moments; these studies are the subject of further investigation.

ASSOCIATED CONTENT

Supporting Information. Crystallographic data for $La_{21-\delta}Mn_8M_7C_{12}$ (M = Ge/Al, Sn, Sb, Te, Bi) and the reinvestigated $La_{21}Fe_8Te_{4.2}Al_{2.8}C_{12}$ structure in the form of CIF files. Tables with atomic coordinates and displacement parameters and Figures S1−S9 (PDF). This material is available free of charge via the Internet at http://pubs.acs.org.

AUTHOR INFORMATION

Corresponding Author

*E-mail: latturne@chem.fsu.edu. Phone: (850) 644-4074. Fax: (850) 644-8281.

Present Addresses

[§]Department of Chemistry, University of Connecticut, U3060, 55 North Eagleville Rd., Storrs, CT 06269-3060.

ACKNOWLEDGMENT

The authors thank Dr. M. Shatruk (Florida State University) for fruitful discussion concerning the magnetism aspects of this work. This research made use of the Scanning Electron Microscope facilities of MARTECH at Florida State University. Financial support from the NSF (Grant DMR-05-47791) is gratefully acknowledged.

REFERENCES

(1) (a) Adachi, G.-Y.; Imanaka, N.; Fuzhong Z. In *Handbook on the Physics and Chemistry of Rare-Earths*; Gschneidner, K. A., Jr., Eyring, L., Eds.; Elsevier: Amsterdam, 1991; Vol. 15. (b) Dashjav, E.; Kreiner, G.; Schnelle, W.; Wagner, F. R.; Kniep, R.; Jeitschko, W. *J. Solid State Chem.* **2007**, *180*, 636. (c) King, B. *J. Organomet. Chem.* **1997**, *536*−*537*, 7. (d) Jeitschko, W.; Gerss, M. H.; Hoffmann, R.-D.; Lee, S. *J. Less-Common Met.* **1989**, *156*, 397. (e) Pöttgen, R.; Jeitschko, W. *Inorg. Chem.* **1991**, *30*, 427. (f) Pöttgen, R.; Jeitschko, W. *Z. Naturforsch.* **1992**, *47b*, 358.

(2) Pecharsky, V. K.; Miller, L. L.; Gschneidner, K. A., Jr. *Phys. Rev. B* **1998**, *58*, 497.

(3) Gerss, M. H.; Jeitschko, W.; Boonk, L.; Nientiedt, J.; Grobe, J.; Moersen, E.; Leson, A. *J. Solid State Chem.* **1987**, *70*, 19.

(4) Scherer, W.; Hauf, C.; Presnitz, M.; Scheidt, E.-W.; Eickerling, G.; Eyert, V.; Hoffmann, R.-D.; Rodewald, U. C.; Hammerschmidt, A.; Vogt, C.; Pöttgen, R. *Angew. Chem., Int. Ed.* **2010**, *49*, 1578.

(5) (a) Gerdes, M. H.; Jeitschko, W.; Wachtmann, K. H.; Danebrock, M. E. *J. Mater. Chem.* **1997**, *7*, 2427. (b) Davaasuren, B.; Borrmann, H.; Dashjav, E.; Kreiner, G.; Widom, M.; Schnelle, W.; Wagner, F. R.; Kniep, R. *Angew. Chem., Int. Ed.* **2010**, *49*, 5688.

(6) Benbow, E. M.; Dalal, N. S.; Latturner, S. E. *J. Am. Chem. Soc.* **2009**, *131*, 3349.

(7) (a) Bramwell, S. T.; Gingras, M. J. P. *Science* **2001**, *294*, 1495. (b) Saunders, T. E.; Chalker, J. T. *Phys. Rev. Lett.* **2007**, *98*, 157201. (c) Andreanov, A.; Chalker, J. T.; Saunders, T. E.; Sherrington, D. *Phys. Rev. B* **2010**, *81*, 014406. (d) Bellier-Castella, L.; Gingras, M. J. P.; Holdsworth, P. C. W.; Moessner, R. *Can. J. Phys.* **2001**, *79*, 1365.

(8) Massalski, T. B.; Okamoto, H. *Binary Alloy Phase Diagrams*, 2nd ed.; ASM International: Materials Park, OH, 1990.

(9) (a) Benbow, E. M.; Dalal, N. S.; Latturner, S. E. *J. Solid State Chem.* **2009**, *182*, 3055. (b) Zaikina, J. V.; Jo, Y.-J.; Latturner, S. E. *Inorg. Chem.* **2010**, *49*, 2773.

(10) *SAINT*; Bruker AXS Inc.: Madison, WI, 2008.

(11) *SADABS*; Bruker AXS Inc.: Madison, WI, 2008.

(12) Sheldrick, G. M. *Acta Crystallogr., Sect. A* **2008**, *64*, 112.

(13) (a) Kleinke, H. *Chem. Mater.* **2010**, *22*, 604. (b) Toberer, E. S.; May, A. F.; Snyder, G. J. *Chem. Mater.* **2010**, *22*, 624. (c) Galadzhun, Ya. V.; Pöttgen, R. *Z. Anorg. Allg. Chem.* **1999**, *625*, 481.

(14) (a) Jepsen, O.; Burkhardt, A.; Andersen, O. K. *The Program TB LMTO-ASA*, version 4.7; Max-Planck-Institut für Festkörperforschung: Stuttgart, Germany, 2000.

(15) Blöchl, P. E.; Jepsen, O.; Andersen, O. K. *Phys. Rev. B* **1994**, *49*, 16223.

(16) $La_{21}Mn_8Sn_7C_{12}$: r(La(1)) = 1.96 Å, r(La(2)) = 2.05 Å, r(La(3)) = 2.20 Å, r(Sn(1)) = 1.88 Å, r(Sn(2)) = 2.69 Å, r(Mn) = 1.22 Å, r(C) = 1.03 Å. $La_{21}Mn_8Sb_7C_{12}$: r(La(1)) = 1.91 Å, r(La(2)) = 2.02 Å, r(La(3)) = 2.13 Å, r(Sb(1)) = 1.86 Å, r(Sb(2)) = 2.68 Å, r(Mn) = 1.23 Å, r(C) = 1.04 Å. $La_{20}Mn_8Te_7C_{12}$: r(La(1)) = 1.88 Å, r(La(2)) = 1.96 Å, r(Te(1)) = 1.96 Å, r(Te(2)) = 2.70 Å, r(Mn) = 1.22 Å, r(C) = 1.04 Å. $La_{21}Mn_8Bi_7C_{12}$: r(La(1)) = 1.92 Å, r(La(2)) = 2.03 Å, r(La(3)) = 2.09 Å, r(Bi(1)) = 1.94 Å, r(Bi(2)) = 2.54 Å, r(Mn) = 1.23 Å, r(C) = 1.04 Å. $La_{21}Mn_8Te_7C_{12}$: r(La(1)) = 1.88 Å, r(La(2)) = 2.04 Å, r(La(3)) = 2.19 Å, r(Te(1)) = 1.86 Å, r(Te(2)) = 2.69 Å, r(Mn) = 1.22 Å, r(C) = 1.03 Å.

(17) Witte, A. M.; Jeitschko, W. *Z. Naturforsch.* **1996**, *51b*, 249.

(18) Zaikina, J. V.; Zhou, H.; Latturner, S. E. *J. Solid State Chem.* **2010**, *183*, 2987–2994.

(19) (a) Kent, R.; Eick, H. *Inorg. Chem.* **1962**, *1*, 956. (b) Weber, F. A.; Schleid, T. *Z. Anorg. Allg. Chem.* **1999**, *625*, 1833.

(20) Steinmetz, J.; Venturini, G.; Roques, B.; Engel, N.; Chabot, B.; Parthé, E. *Acta Crystallogr., Sect. B* **1982**, *38*, 2103.

(21) Stepień-Damm, J.; Shlyk, L.; Suski, W.; Wochowski, K. *J. Alloys Compd.* **1995**, *224*, 225.

(22) Tkachuk, A. V.; Crerar, S. J.; Mar, A. *J. Solid State Chem.* **2004**, *177*, 3939.
(23) Kahnert, G. E.; Jeitschko, W.; Block, G. *Z. Anorg. Allg. Chem.* **1993**, *619*, 442.
(24) Kahnert, G. E.; Jeitschko, W. *Z. Anorg. Allg. Chem.* **1993**, *619*, 93.
(25) Böcker, U. A.; Jeitschko, W.; Block, G. *J. Alloys Compd.* **1996**, *236*, 58.
(26) The crystal structure refinement of $La_{21}Fe_8Te_{4.2}Al_{2.8}C_{12}$ was reinvestigated, and the partial occupancy of the La(3) site was found; the new CIF file is provided in the Supporting Information (CSD 260241).
(27) (a) Besnus, M. J.; Herr, A; Le Dang, K; Veillet, P.; Schaafsma, A. S.; Vincze, I.; van der Woude, F.; Mezei, F.; Calis, G. H. M. *J. Phys. F: Met. Phys.* **1982**, *12*, 2393. (b) Ijjaali, I.; Welter, R.; Venturini, G.; Malaman, B.; Ressouche, E. *J. Alloys Compd.* **1998**, *270*, 63. (c) Motizuki, K.; Korenari, T.; Shirai, M. *J. Magn. Magn. Mater.* **1992**, *104*, 1923. (d) Xia, S. Q.; Myers, C.; Bobev, S. *Eur. J. Inorg. Chem.* **2008**, *27*, 4262.
(28) Mydosh, J. A. *Spin Glasses: An Experimental Introduction*; Taylor and Francis: London, 1993.
(29) Long, G. J.; Hautot, D.; Mohan, A.; Hughbanks, T.; Xie, X.; Grandjean, F. *J. Am. Chem. Soc.* **1998**, *120*, 12163.
(30) (a) Al-Qadi, K.; Wang, P.; Stadnik, Z. M.; Przewoźnik, J. *Phys. Rev. B* **2009**, *79*, 224202. (b) Chi, J.; Li, Y.; Vagizov, F. G.; Goruganti, V.; Ross, J. H. *Phys. Rev. B* **2005**, *71*, 024431.
(31) (a) Niepmann, D.; Pöttgen, R.; Künnen, B.; Kotzyba, G.; Rosenhahn, C.; Mosel, B. D. *Chem. Mater.* **1999**, *11*, 1597. (b) Hoffmann, R.-D.; Kussmann, D.; Rodewald, U. C.; Pöttgen, R.; Rosenhahn, C.; Mosel, B. D. *Z. Naturforsch.* **1999**, *54b*, 709.
(32) Leithe-Jasper, A.; Rogl, P.; Wiesinger, G.; Rainbacher, A.; Hatzl, R.; Forsthuber, M. *J. Magn. Magn. Mater.* **1997**, *170*, 189.
(33) Lippens, P. E. *Phys. Rev. B* **1999**, *60*, 4576.